Journal of Applied Polymer Science

Flow-induced solidification of high-impact polypropylene copolymer compositions: Morphological and mechanical effects

Martin van Drongelen,[1] Markus Gahleitner,[2] Anne B. Spoelstra,[3] Leon E. Govaert,[1] Gerrit W. M. Peters[1]

[1]Department of Mechanical Engineering, Materials Technology Institute, Eindhoven University of Technology, 5600 MB, Eindhoven, the Netherlands

[2]Borealis Polyolefine GmbH, Innovation Headquarters, St. Peterstr. 25, 4021 Linz, Austria

[3]Department of Chemical Engineering and Chemistry, Laboratory of Polymer Technology, Eindhoven University of Technology, 5600 MB, Eindhoven, the Netherlands

Correspondence to: G. Peters (E-mail: g.w.m.peters@tue.nl)

ABSTRACT: Polypropylene-based impact copolymers are a complex composition of matrix material, a dispersed phase and many optional modifiers. The final heterophasic morphology of such systems is influenced significantly by the processing step, adding an additional level of complexity to understanding the structure-property relation. This topic has hardly been studied so far. The effect of thermal history and shear flow on the solidification process of three different compositions of a polypropylene-based impact copolymer, i.e., one base material and two compounds with either high density polyethylene or ethylene-*co*-octene added, is investigated. Samples are examined using differential scanning calorimetry, extended dilatometry, transmissions electron microscopy, and finally, tensile testing. With flow, the materials show pronounced flow-enhanced crystallization of the matrix material and deformed filler content. Compared to the base polymer, the stress–strain response of the compounded samples shows a lower yield stress and more pronounced influence of shear, reflected in the increasing strain hardening modulus. © 2015 Wiley Periodicals, Inc. J. Appl. Polym. Sci. **2015**, *132*, 42040.

KEYWORDS: blends; copolymers; crystallization; mechanical properties; structure-property relations

Received 18 November 2014; accepted 28 January 2015

DOI: 10.1002/app.42040

INTRODUCTION

Advanced polypropylene (PP) materials are extensively being used for automotive parts like bumpers, body panels, dashboards and door claddings for many years. However, with increasing requirements in areas like advanced packaging and non-pressure pipes these grades find more and more applications. Mostly, heterophasic blends with crystalline PP as the continuous phase and an amorphous ethylene-propylene copolymer (EPR) as disperse phase, produced in multi-stage polymerization processes, are used.[1–3] The PP matrix delivers the stiffness of the material whereas the rubbery inclusions act as impact modifiers. Thus, a material with balanced stiffness-impact behavior and even good optical performance can be obtained. When designing the property balance of such systems, multiple variations of the components are possible, which normally require significant resources in either bench scale or pilot-scale synthesis. An alternative for exploring a wide composition range with limited efforts is the production of model compounds, in which the phase structure of reactor-based systems needs to be matched as close as possible, including the frequent presence of a crystalline polyethylene (PE) component.[4–8] The latter can be used either for generating model systems for reactor-based products[5] or for property modification of these high-impact copolymers. Requirements for which the presence of crystalline PE in significant amounts has been found advantageous are limitation of stress whitening[9,10] and scratch resistance,[11] both being highly relevant e.g., for automotive interior applications. In any case, the morphology of such high-impact systems will be influenced significantly by the product shaping process, adding a further level of complexity to the crystal structure in PP. While many papers deal with the effect of polymer composition on the equilibrium morphology of high-impact copolymers (i.e., as solidified from a quiescent melt),[3,12,13] the consequences for the morphology and the related mechanical performance in injection-moulded parts have been hardly studied. The limited number of publications dealing with morphological structures in injection-molded or otherwise processed parts from PP/EPR model or reactor-based

systems are mostly restricted to one composition[14,15] or one set of processing conditions.[16,17] In contrast to this limitation, significant progress has been made in recent years in understanding the effect of composition variations,[18,19] nucleation,[20] and processing parameters[21,22] on the crystal structure and the resulting mechanical performance of single-phase PP homopolymers or random copolymers. An extended dilatometer, an experimental setup to study pressure-volume-temperature (PVT) behavior with variable cooling rate and a well defined shear history, used in some of these cases,[18,21] has been applied in the present study for studying three high-impact PP copolymer compositions under processing-relevant conditions. The objective of the investigation was to extend the understanding of the interaction between crystallization, phase structure formation and the mechanical properties of such systems as a function of cooling rate and flow conditions.

We systematically investigated three different compositions of a PP-based impact copolymer, i.e., one base material and two compounds with either high density polyethylene or ethylene-*co*-octene added. Samples were examined using differential scanning calorimetry, extended dilatometry, transmissions electron microscopy and, finally, tensile testing. Flow conditions up to 180 1/s were examined, which is not of the magnitude of maximum shear rates (1000 1/s) but comparable to average shear rates as found in injection molding. Moreover, this range of shear rates was found to cover the full range of solidification regimes. With flow, the materials showed pronounced flow-enhanced crystallization of the matrix material, including shish-kebab formation for strong enough flow. For such strong flow conditions, and especially for the compounded materials, this was accompanied by heavily stretched amorphous particles. Compared to the base polymer, the stress–strain response of the compounded samples showed a lower yield stress and more pronounced influence of shear. With flow, the yield stress and strain hardening modulus, measured in the direction of flow, increased according to the orientation of the matrix and filler content. For the strongest flow conditions, the severely deformed rubber inclusions no longer enhance the ductility of the material, ultimately leading to brittle failure of the specimens.

MATERIALS AND METHODS

Materials

A commercial EP copolymer of Borealis from a multistage polymerization process based on a 4th generation Ziegler-Natta catalyst was used as base material. The grade has a melt flow rate (MFR, ISO 1133, 230°C/2.16 kg) of 10 g/10 min, an EPR content expressed as the xylene cold solubles content of 12.5 wt % and a total ethylene content of 8.3 wt %. Two commercial PE grades were used for modification of this base grade.

- High density polyethylene (HDPE) PE BS4641 of Borealis with an MFR (190°C/2.16 kg) of 0.7 g/10 min and a density of 964 kg/m3, and
- Ethylene-co-octene plastomer (EOC) Engage EG8100 of Dow Chemical with an MFR (190°C/2.16 kg) of 1.0 g/10 min and a density of 870 kg/m3.

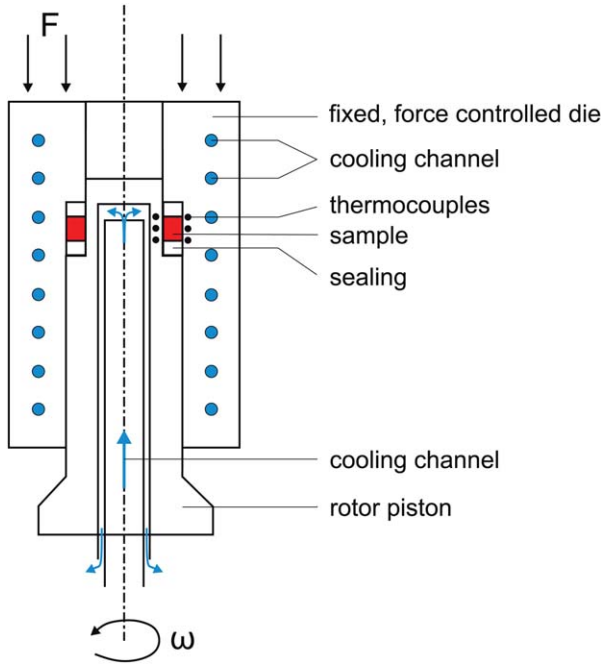

Figure 1. Working principle of the Pirouette. [Color figure can be viewed in the online issue, which is available at wileyonlinelibrary.com.]

This combination was selected because the melt viscosity of the modifiers is very similar to the EPR phase in the base polymer (as also expressed by the intrinsic viscosity). Seventeen weight percentage of each modifier was blended in a twin-screw extruder (ThermoPrism TSE24) at 200–240°C, running the base polymer through the extruder as well to ensure an identical thermal history. Thus, a total of three materials were investigated, a base material, abbreviated as EP/EPR, and two model compounds with HDPE and EOC content, abbreviated as EP/EPR/HDPE and EP/EPR/EOC, respectively.

Methods

Thermal Analyses. Differential scanning calorimetry (DSC) analysis was employed to characterize the melting and crystallization behaviour of the different materials using a Mettler-Toledo 823e/700 module. The sample was heated with 10°C/min from 25°C to 210°C, held at that temperature for 5 min and subsequently cooled at the same rate to 25°C and, after 1 min to ensure stable starting conditions, again heated to 210°C. For each experiment, the recorded heat flow was normalized by sample mass.

Dilatometry. To examine the influence of various processing conditions on the solidification process of the different materials, dilatometry experiments were performed with the Pirouette $PVT\dot{T}\dot{\gamma}$ apparatus (IME technologies, the Netherlands).[18,21] It allows investigation of the evolution of specific volume of polymers as a function of temperature, pressure, cooling rate, and shear rate by measuring the volume change of a sample. A schematic overview of the most important components is shown in Figure 1.

The apparatus requires ring-shaped samples with a mass of 75 mg, an outer diameter of 20 mm, thickness of 0.5 mm, and

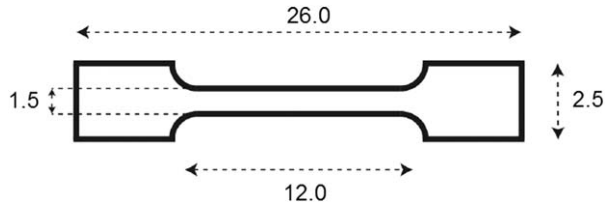

Figure 2. Dimensions of tensile bars in mm.

height of ~2.5 mm, which were preproduced from granular material using a Babyplast injection molding machine (Rambaldi, Italy) equipped with a custom build mold. All experiments were performed in isobaric cooling mode at a pressure of 100 bar. The sample was heated to 220°C and kept at that temperature for 10 min to erase all thermal history. Finally, the piston and die were cooled by either natural convection or a constant flux of air or water, which resulted in initial cooling rates of about 0.1, 1.0, and 90°C/s, respectively. Cooling rates were determined as the temperature gradient between 195 and 130°C. Experiments with flow were carried out during air cooling for different shear rates (3, 10, 30, 60, 100, and 180 s^{-1}), at a constant shear time of 1 s at set shear temperature of 138°C. Directly after the experimental run, samples were removed from the apparatus and stored in a freezer at −18°C for later structure analysis.

Transmission Electron Microscopy. Samples for transmission electron microscopy (TEM) were trimmed from processed dilatometry samples perpendicular to the shear direction at low temperature (−120°C) using a Diatome trimming tool. Subsequently, samples were stained for 24 h with a RuO_4 solution prepared according to Montezinos *et al.*[23] Ultrathin sections (70 nm) were obtained at −100°C using a Leica S/FCS microtome equipped with a Diatome 35° knife. The sections were put on a 200 mesh copper grid with a carbon support layer and examined in a Tecnai 20 transmission electron microscope, operated at 200 kV.

Mechanical Characterization. Mechanical properties were investigated by uniaxial tensile experiments in general accordance with ISO 527 using a Zwick Z010 universal tensile tester, equipped with a 100 N load cell and at a strain rate of 10^{-3} s^{-1}. Two dogbone shaped, 0.5 mm thick samples were cut from each PVT-sample in order to execute all experiments in duplo, other dimensions of the specimen are given in Figure 2.

Before starting the actual experiment, a preload of 0.2 MPa was applied at 1 mm/min. All experiments were performed at room temperature (23°C) and two weeks after sample removal from the freezer to prevent any influence of physical ageing. From the tensile test, both yield stress, σ_y and strain hardening modulus, G, were determined as macroscopic phenomena from which to characterize the influence of flow on the final mechanical properties of the sample. Here, σ_y is determined from the tensile curves using the secant method as described by Ward,[24] and G from the slope of the true stress versus the neo-Hookean strain measure at large deformation. In the case of (preyield) brittle failure, the strain hardening modulus could not be determined. Impact and flexural (3-point bending) testing was performed using 80 × 10 × 4 mm^3 test bars, injection molded in line with EN ISO 1873-2 (melt temperature 200°C, mold temperature 40°C). A 3-point flexural test according to ISO 178 (+23°C) and Charpy notched impact test according to ISO 179 1eA (+23°C and −20°C) was performed in line with general industrial practice. Also, the melt flow rate (MFR) was measured according to ISO 1133 (230°C, 2.16 kg load).

RESULTS AND DISCUSSION

The effect of processing conditions on the final morphology and mechanical properties of the three materials was investigated. First, the melting and crystallization behaviour was characterized using DSC and using extended-dilatometry at different cooling rates. The influence of flow was investigated by imposing a one second shear pulse at a constant temperature and different shear rates during intermediate cooling. The final morphology was visualized using TEM for samples processed at three selected shear rates. Finally, mechanical properties were examined as a function of shear using tensile tests.

Melting and Crystallization Behavior

The effect of material composition on melting/crystallization behaviour of the materials was evaluated. The data recorded during the second heating and first cooling run are shown in Figure 3. For all materials, a clear melting peak of the EP matrix is recognized at 165°C. In addition, a small endotherm is seen at 120°C, which can be attributed to the small amount of PE present in the material. For the EP/EPR/HDPE, this peak partially overlaps with melting of the HDPE content, with the peak maximum observed at 131°C; it can be clearly observed as a shoulder on the HDPE melting peak. Regarding the compound with added EOC, a broad melting peak is found around 60°C, which is typical for ethylene copolymers with higher amounts of longer alpha-olefins as comonomer.[25] On cooling, data shown in Figure 3(b), all materials show one clear crystallization peak, which indicates that, for the current thermal conditions, crystallization of the matrix components occurs at similar temperatures (124, 119, and 120°C). Small exotherms are observed at ~100 and 45°C because of crystallization of the polyethylene fraction and the EOC modifier, respectively. No crystallization peak of the HDPE modifier can be distinguished separately from the matrix peak since the crystallization temperatures of these components overlap.[26]

The effect of thermal history was further investigated in terms of (specific) volume rather than in terms of heat flow. These are the base results to compare with when studying the influence of flow. Moreover, by comparing to DSC results we show that the dilatometer results are consistent. Dilatometry experiments were performed at three different cooling rates, all at an isobaric pressure of 100 bar. By measuring the expansion or shrinkage of the sample, the specific volume, v, can be plotted as function of temperature, see Figure 4. Three different regions can be identified during cooling; the melt, crystallization, and solid regime, from high to low temperature, respectively. The presence of the ethylene-based content in the base material is recognized throughout the entire dataset by the lower specific volume of both compounds. The crystallization temperature, T_c,

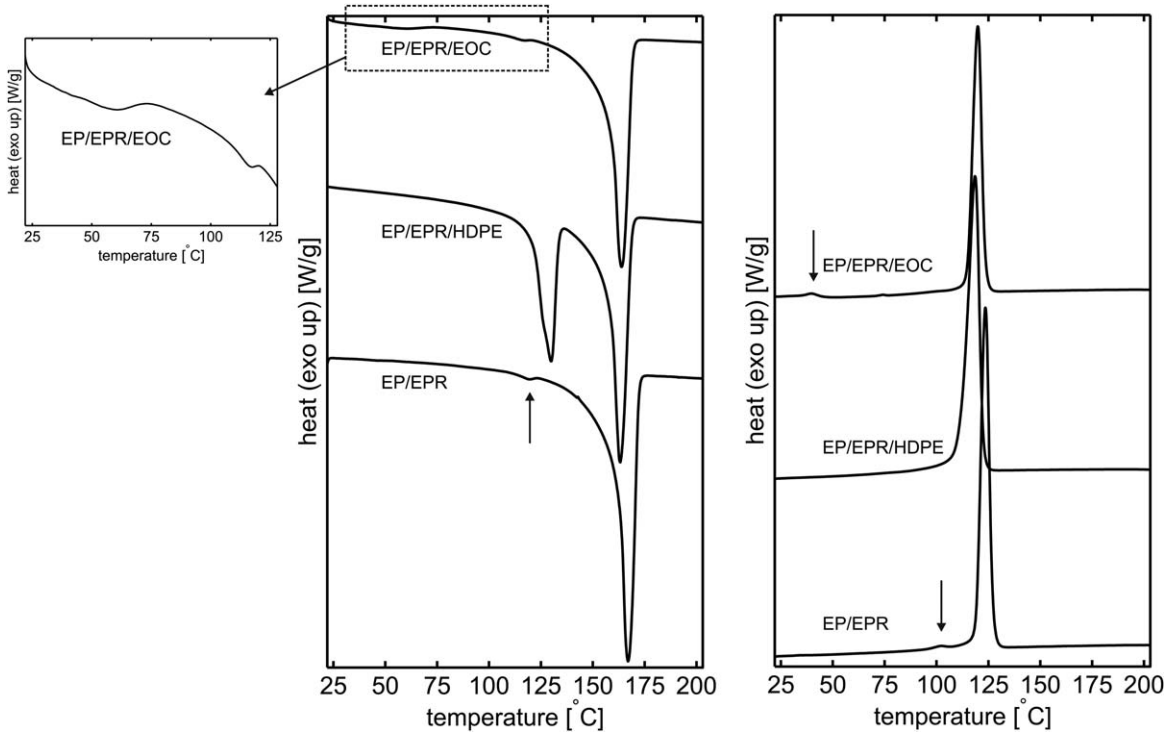

Figure 3. DSC traces of second heating with zoomed in detail of the low temperature region for EP/EPR/EOC (left) and first cooling (right) for all materials investigated. Cooling rate investigated is 10°C/min (0.17°C/s).

is determined halfway between the melt and solid stage regime and presented for all materials and conditions in Table I. The dilatometer results for the lowest cooling rate (0.1°C/s) are consistent with those found with DSC (0.17°C/s). With cooling rate, the crystallization regime spreads out over a larger temperature window, and consequently, T_c decreases. Because of the higher cooling rate, the process of nucleation and crystal growth is shifted towards a lower temperature, a common observation in non-isothermal crystallization studies.[27] For the two lowest cooling rates, the components of the different materials show, in agreement with the results from DSC, only one pronounced crystallization region. Here, crystallization of the PE content is not or only very weakly observed in terms of dilation. At the highest (initial) cooling rate of 90°C/s, minor signs of a second crystallization process can be observed around 80°C, which can be attributed to the polyethylene content of the EP/EPR and EP/EPR/HDPE material, Figure 4(a,b), respectively. Crystallization of PE in the EP/EPR/EOC compound could not be detected for this cooling rate.

Effect of Flow

Similar to the method explored by van Erp *et al.*,[28] the influence of the thermomechanical history during cooling was investigated by applying flow as a step function of 1 s in a range of shear rates (3–180 s^{-1}). Air was used for cooling (~1°C/s) to provide a narrow temperature window during the shear pulse. In this study, the shear temperature, $T\dot{\gamma}$, was chosen equal for all materials and investigated at a fixed temperature of 30°C below the pressure corrected melting temperature, T_m (p), of the PP matrix. $T\dot{\gamma}$ is defined as:

$$T\dot{\gamma} = T_m(p_0) + \kappa(p - p_0) - \Delta T,$$

where κ is the pressure shift factor of 3°C/100 bar, assumed similar to isotactic PP,[29] p_0 is the atmospheric pressure in bar, and ΔT the level of undercooling, set to 30°C. Since the melting temperature was determined by DSC (10°C/min) at 165°C, $T\dot{\gamma}$ was set at 138°C. This level of undercooling was chosen such that get clear but not too strong effects of the flow applied. All experiments were performed at an elevated pressure of 100 bar. Dilatometry is a convenient way to study the influence of pressure on the crystallization kinetics. However, here we will focus on the effect of flow. To easily compare the influence of different thermomechanical histories on the crystallization process, rather than to focus on the absolute value of the specific volume, the raw data is converted in a normalized specific volume, v^*, using:

$$v^* = \frac{v - v_s}{v_m - v_s}$$

where v is the measured specific volume, v_s the specific volume in the solid state at 40°C and v_m is the specific volume in the melt at 200°C.

EP/EPR Base Material. The effect of flow on the evolution of the normalized specific volume is plotted for EP/EPR in Figure 5. The influence of flow is clear; with increasing shear rate, the crystallization temperature increases with as much as 20°C. As a result of the applied flow, the molecules are arranged in flow direction, decreasing the melt entropy, thus increasing the driving force for crystallization. Molecular orientation stimulates the formation of flow induced nuclei, which depending on the conditions, can tremendously increase the rate of crystallization.[30]

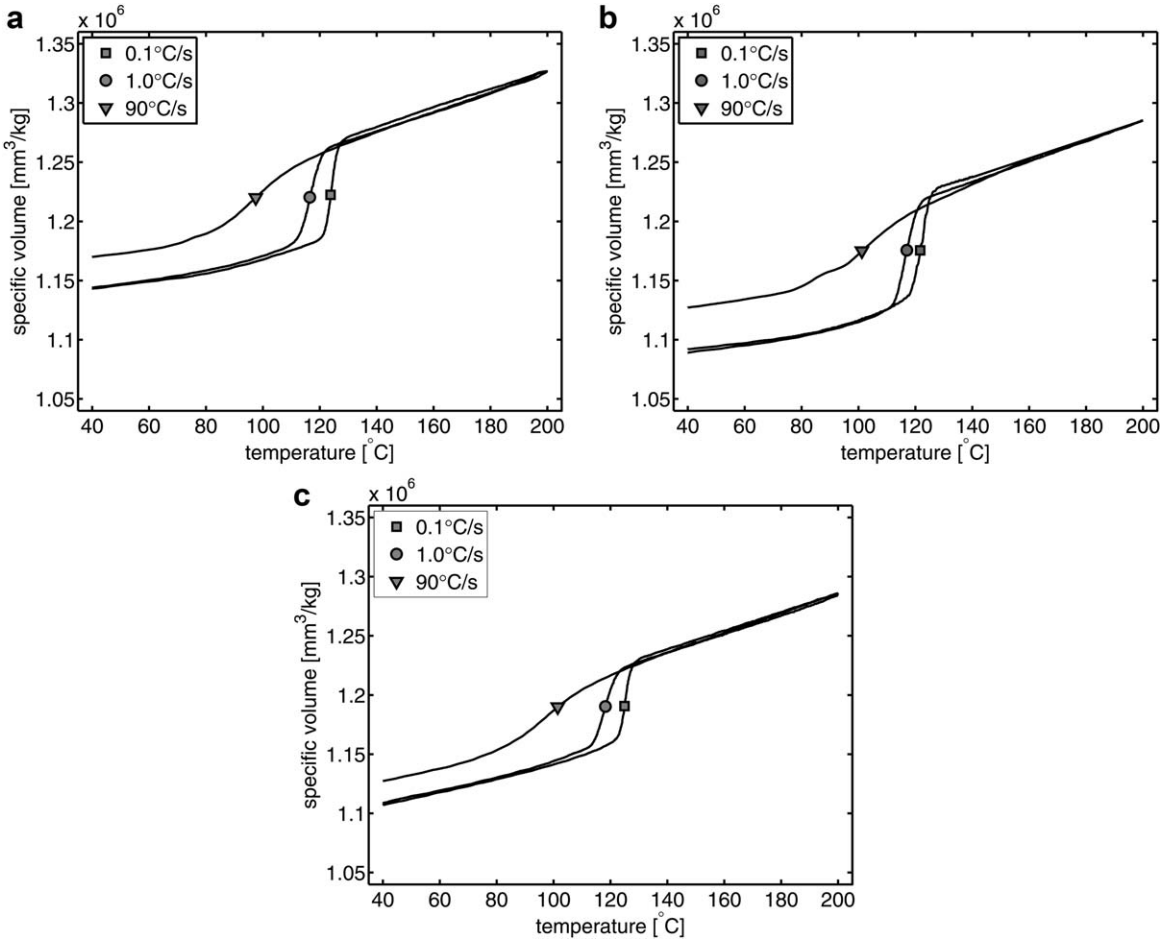

Figure 4. Effect of cooling rate on the specific volume evolution of the (a) EP/EPR copolymer, (b) EP/EPR/HDPE compound and (c) the EP/EPR/EOC compound.

The difference between the quiescent case and the lowest shear rate (3 s^{-1}) condition is hardly noticeable. At the highest shear rate (180 s^{-1}), the crystallization temperature equals the shear temperature, which evidences a very high crystallization rate and formation of flow-induced structures.[28] Obviously, upon a further increase of the shear rate, the crystallization temperature can never exceed the shear temperature. Note the "dip" in the data at the shear temperature of 138°C, this is an experimental error due to the sudden movement of the rotor piston inside the Pirouette and is further ignored.

The phase structure of heterophasic PP impact copolymers is determined by three main factors: the viscosity ratio between the matrix and elastomer, phase compatibility and the deformation history during processing.[3,5,8,26] Since both the viscosity and phase compatibility are predetermined factors by the choice of (compounded) material, the structure was studied as a function

Table I. Crystallization Temperatures from Dilatometry and DSC at Different (Initial) Cooling Rates

Composition	EP/EPR	EP/EPR/HDPE	EP/EPR/EOC
0.1 (°C/s)	123.8	121.7	125.0
1.0 (°C/s)	116.5	117.0	118.2
90.0 (°C/s)	97.5	101.2	101.5
0.17 (°C/s) (DSC)	123.5	118.5	119.9

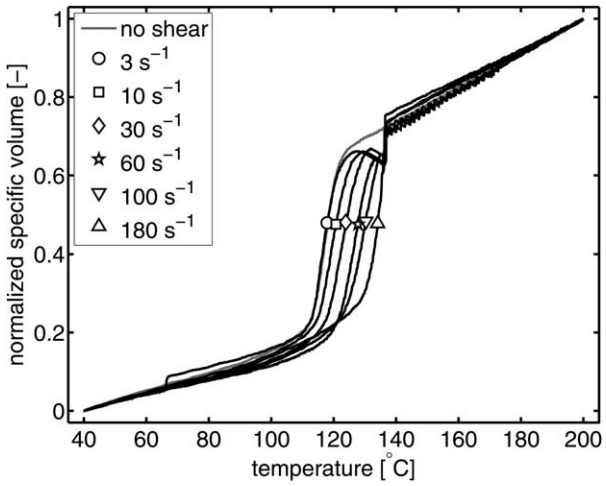

Figure 5. Effect of shear flow on the normalized specific volume evolution of EP/EPR.

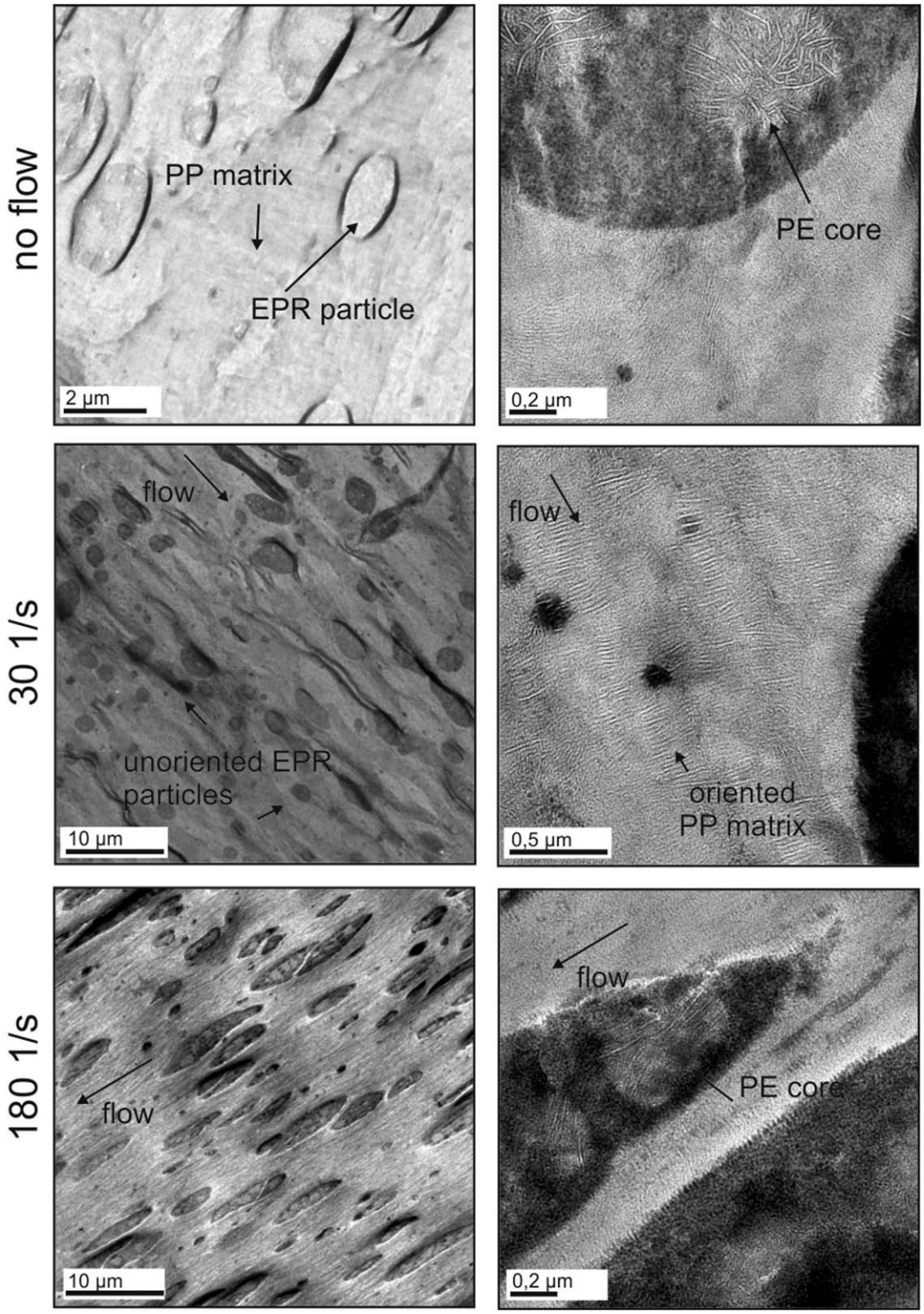

Figure 6. TEM micrographs of the morphology after solidification without flow (top), with intermediate flow (middle) and strong flow (bottom) of the EP/EPR material in low detail (left column) and high detail (right column). PE inclusions are recognized inside the modifier. With flow, oriented lamellae are formed in the matrix perpendicular to flow direction. After strong flow, the modifier remains slightly stretched in the oriented matrix.

of the thermal and deformation history only, taking the sample crystallized in quiescent conditions as a reference state. Where earlier work on these materials focuses on the particle size distribution or the interaction between the different components,[8,26] we will focus only on the effect of flow on the final morphology and the mechanical properties thereof (next section).

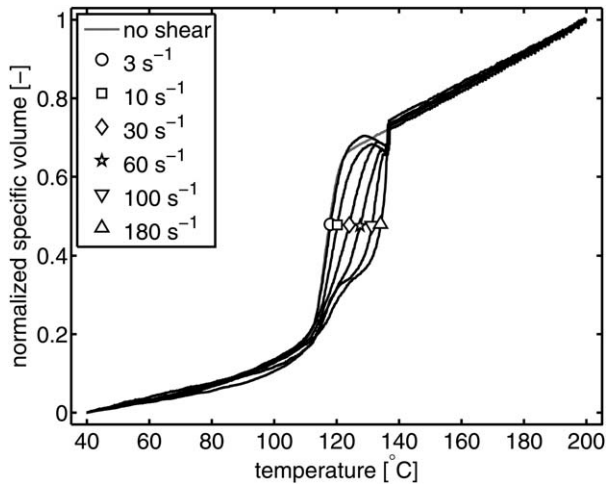

Figure 7. Effect of shear flow on the normalized specific volume evolution of the EP/EPR/HDPE compound.

To visualize the final morphology, detailed TEM pictures were taken on 70 nm thick coupes cut in the vorticity direction. Samples crystallized from the melt in quiescent conditions, with intermediate flow strength (30 s^{-1}) and strong flow (180 s^{-1}) were examined, see Figure 6. High- and low-detail pictures, representative for the entire sample, were selected for each condition. The matrix material shows a spherulitic PP structure in which amorphous EP regions are dispersed.[31] Inside the modifier, multiple crystalline PE inclusions are located, recognized by bright lamellae, designating the dispersed phase as a core-shell particle. It is known that with increasing ethylene concentration, the amorphous particles become larger and may possess several crystalline inclusions, also known as salami-particles.[32,33] Here, the amount of ethylene is sufficient to form a number of inclusions in each EPR domain.

Upon intermediate flow conditions, flow-enhanced features can be observed such as a number of lamellae that have grown perpendicular to the direction of flow (kebabs). Meanwhile, the modifier content remains unoriented. A stretched EPR particle can be considered as a deformed and confined viscoelastic droplet, which may relax to a spherical particle, depending on the ratio between interfacial forces and viscosities.[34] If the relaxation process is slow, the particle remains stretched on solidification, alternatively, it relaxes back to the original shape. The exact parameters for this relaxation process are not known for this system. However, we have explored a sufficient large range of shear rates to cover the full range of deformed EPR particles. The effect of strong flow conditions, displayed in the bottom half of Figure 6, is best noticed through the particle anisotropy. The matrix material also shows an increased level of orientation, which can be deduced from the alternating light and dark bands found perpendicular to the direction of flow. Inside the EPR shell, the PE inclusions remain unoriented and still appear in the spherulitic confirmation. Because of the high $T\dot{\gamma}$ with respect to the melting point of PE, the PP matrix orients upon flow and crystallizes ahead of the small percentage of ethylene within the EPR regions.

EP/EPR/HDPE Compound. The same experimental protocol was applied for the EP/EPR/HDPE compound. Upon low shear conditions, the results in Figure 7 are similar to those in Figure 5; flow only increases the crystallization temperature with a few degrees. However, upon strong flow conditions, e.g. 60 s^{-1} and above, crystallization is completed in a two step process. Here, the first crystallization process starts during or directly after the shear pulse and is completed at a temperature of ~130°C. It is not before the end of the second crystallization process, which sets in around 120°C, that space filling is complete and v^* overlaps the solid regime data of the unsheared sample.

Since the material investigated is a multicomponent system, each component having different crystallization kinetics, the multiple volume fractions will crystallize at different temperatures. In the absence of flow and for the lowest shear rates, crystallization of the matrix component overlaps with crystallization of the HDPE component, as observed in DSC and dilatometry, Figures 3 and 4(b), respectively. For higher shear rates, the first crystallization process at higher shear rates is attributed to flow-induced crystallization of the matrix material. Since, $T\dot{\gamma}$ is well above the melting temperature of HDPE, it is assumed the relaxation times of this component are relatively short and the molecules are able to relax after flow. Still, crystallization of the HDPE component is slightly enhanced with flow, i.e., crystallization of the second process shifts towards higher temperatures. It is expected that the heavily oriented PP matrix acts as a nucleating surface for the crystals formed by the HDPE, a detail which could be extracted from the TEM pictures in Figure 8.

The morphology of the unsheared sample shows EPR shells that contain a (high-density) polyethylene core, which itself, in some cases, contains an amorphous section with again an ethylene core. The HDPE (and ethylene from the base material, it is not possible to distinguish between the two) form distinct lamellae, which are situated mostly within the amorphous regions. A significant number of lamellae have grown from the matrix inside the shell or vice versa, and are expected to increase the adhesion level between matrix and modifier particle. Opposite to the TEM pictures of EP/EPR, a small number of thick PE lamellae can also be recognized within the PP matrix as a result of the partial miscibility of the components.[8]

At intermediate flow conditions, TEM reveals a slightly oriented matrix and modifier content. After flow, most rubber inclusions are not able to relax, most probably due to the high adherence level, or compatibility, between matrix and particle with HDPE content.[8,12,26] Most intriguing is the morphology of the strongly sheared samples; heavily oriented features were obtained, where the EPR particles are stretched throughout the matrix. The HDPE content is still recognized as the most light regions, mainly located at the edge of the amorphous zones. When examined in high detail, shish-kebab structures can be seen clearly in the matrix section. Any misalignment of the shish with the flow direction is expected to be caused by preparation of the fragile ultra-thin sample coupes. The HDPE fractions are always located inside the EPR particles and, most importantly, found adjacent to the PP shish-kebabs, which provide the HDPE lamellae with a suitable growth surface, assumed responsible for the somewhat higher crystallization temperature in dilatometry measurements, Figure 4(b). This is compatible with results for iPP/PE blends, where the PE fraction was found to

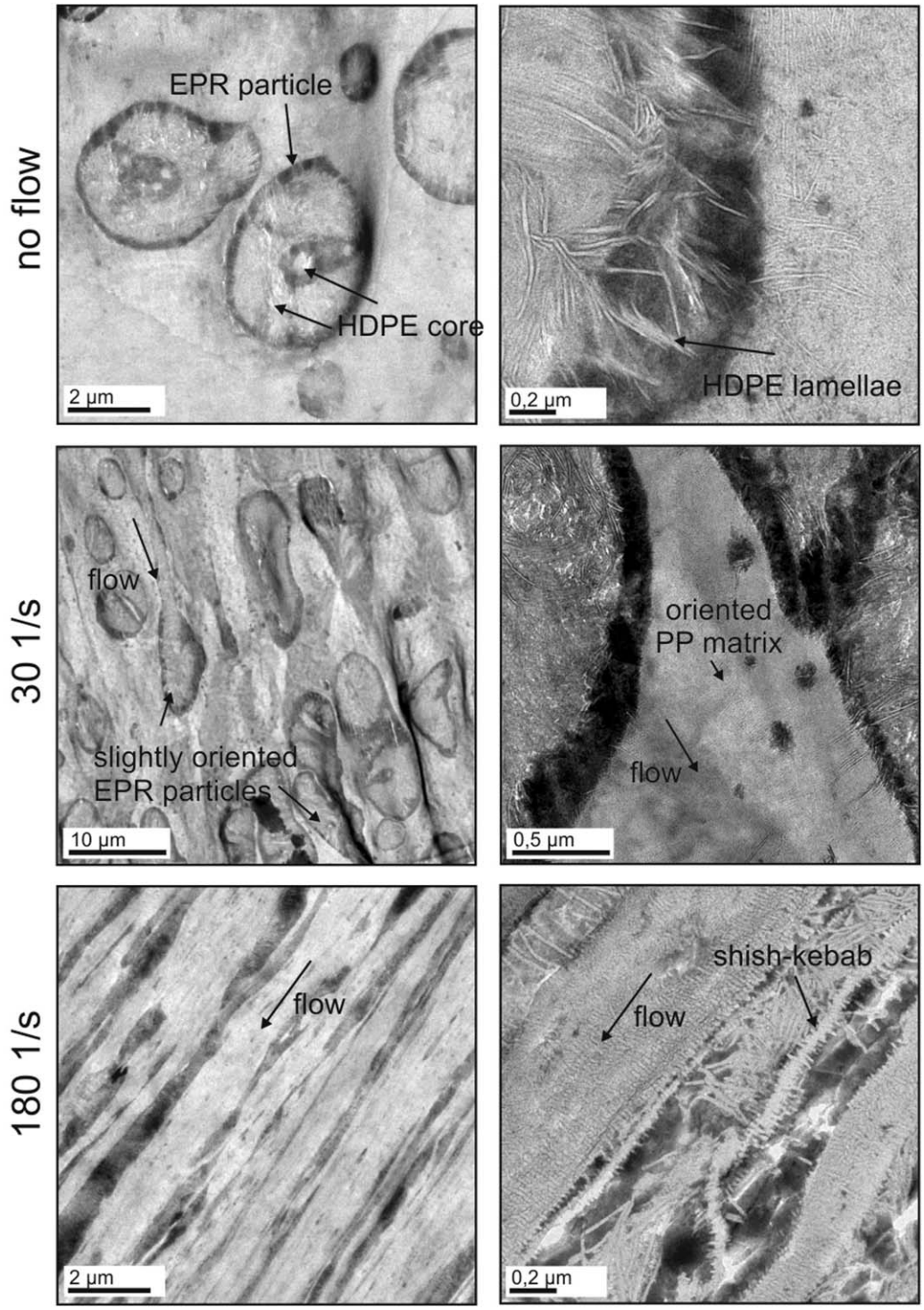

Figure 8. TEM micrographs of the morphology after solidification without flow (top), with intermediate flow (middle) and strong flow (bottom) of the EP/EPR/HDPE material in low detail (left column) and high detail (right column). PE lamellae are recognized at the modifier boundary. With medium flow, oriented lamellae are formed in the matrix perpendicular to flow direction, while the modifier particles remain un-oriented. After strong flow conditions, the matrix and modifier are fully oriented and shish-kebab structures can be observed from the matrix.

epitaxially crystallize on an oriented crystalline iPP interface, which generated an increased number of nuclei.[35–37]

EP/EPR/EOC Compound. Finally, the EP/EPR/EOC compound is investigated for varying thermomechanical histories. From the results presented in Figure 9, it is clear that, once more, crystallization of the matrix component is severely enhanced with flow. For the two highest shear rates, nearly identical crystallization kinetics are observed. Here, the strength of flow is such that, already at 100 s^{-1}, crystallization starts during the shear

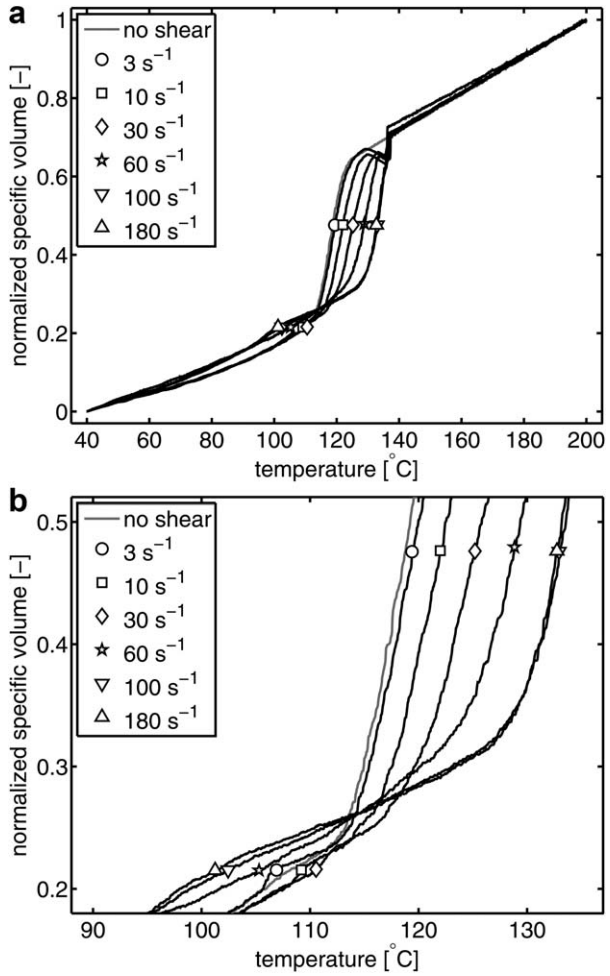

Figure 9. (a) Effect of shear flow on the normalized specific volume evolution of the EP/EPR/EOC blend and (b) a zoom-in on the temperature region of the second crystallization process.

pulse and the shift of T_c reaches its maximum. With increasing shear rate, a small shoulder in the specific volume evolution is present around 110°C as a result of the fraction crystallizing at these low temperatures only. Because of data overlap at low temperatures, it is hard to distinguish between the different curves and a more detailed picture of the 90–130°C temperature window is presented in Figure 9(b). From the DSC data (taking into account a shift of ~3°C in T_c due to the pressure difference) it is evident that this shoulder concerns crystallization of the polyethylene content within the base material. The EOC will crystallize at a later stage, i.e., at a much lower temperature of ~60°C.

For the 100 and 180 s^{-1} shear rate, and to a smaller extend for 60 s^{-1}, a higher specific volume is obtained after crystallization of the matrix and, subsequently, the shoulder is shifted to temperatures around 100°C. From the dilatometry data alone, it is difficult to explain this phenomena. Therefore, we first investigate the morphology as visualized by TEM, Figure 10.

In contrast to EP/EPR/HDPE, see Figure 8, the EOC compound does not form visible crystalline lamellae within the particles. In fact, it is not possible to recognize the EOC in the TEM micrographs. A large part of the EOC content is dissolved in the amorphous regions, enabled by the partial miscibility between both components.[8,26] Moreover, upon high concentrations of (long-chain) branching content, literature reports on EOC to "order" in so-called fringed-micellae or bundle-like structures,[25,38] which are hard to distinguish using TEM. The lamellae that are visible in the high-detail picture of the unsheared sample, originate from the ethylene content in the base material, see also Figure 6. Similar to the other materials investigated, the intermediate shear rate only induces an oriented matrix and does not or only weakly affect the filler particles. The influence of EOC content on the morphology displayed in the bottom of Figure 10 is severe, especially when the sheared base material is taken as a reference (Figure 6). TEM reveals heavily deformed EPR/EOC particles among with the embedded crystalline PE. In high-detail, flow-induced PP structures are found in the matrix amidst the amorphous regions. Although we cannot draw any strong conclusions regarding the shift of the shoulder found with dilatometry, it is expected that (flow-induced) crystallization of the matrix and ethylene content are suppressed by the long-chain branched EOC which is partly dissolved in the EPR particles and acts as tie-chains. With flow, the EOC content will be distributed throughout the matrix; with an increase of topological constraints (knots, ties) collecting suitable crystallizing chain sequences to the crystal front (or rejecting branches from crystals) is slowed down[39]; hence, crystallization, an increase of the overall density, is measured at a lower temperature.

Mechanical Properties

For each of the three heterophasic copolymers investigated, the components and the final morphology play a decisive role during deformation. Extensive work in this field has been performed by Bucknall[40] and by Kim and Michler *et al.*,[32,41,42] of whom the latter categorized a number of micromechanical deformation mechanisms for a range of filled polymer compounds using combined electron microscopy and *in situ* tensile testing. In general, a three-stage mechanism is present for particle filled semi-crystalline systems:

- Stress concentration of the modifier: Because of the different elastic properties, the particles act as stress concentrators, which leads to the development of a tri-axial stress inside these particles.
- Void and shear band formation: Build-up of high stress concentrations induces void formation through cavitation inside the particles or due to debonding at the particle matrix interface. At the same time, weak shear bands are formed between the voids.
- Induced shear yielding: After cavitation or debonding, stress is locally released into the matrix, increasing the shear component and inducing shear yielding.

A standard characterization of the different materials used was performed. Table II summarizes the mechanical performance of materials as tested under standard impact and bending conditions. The HDPE addition results only in a limited stiffness reduction, with positive impact strength effects at ambient and sub-zero temperatures. In contrast, the EOC addition reduces the stiffness significantly while boosting impact strength much

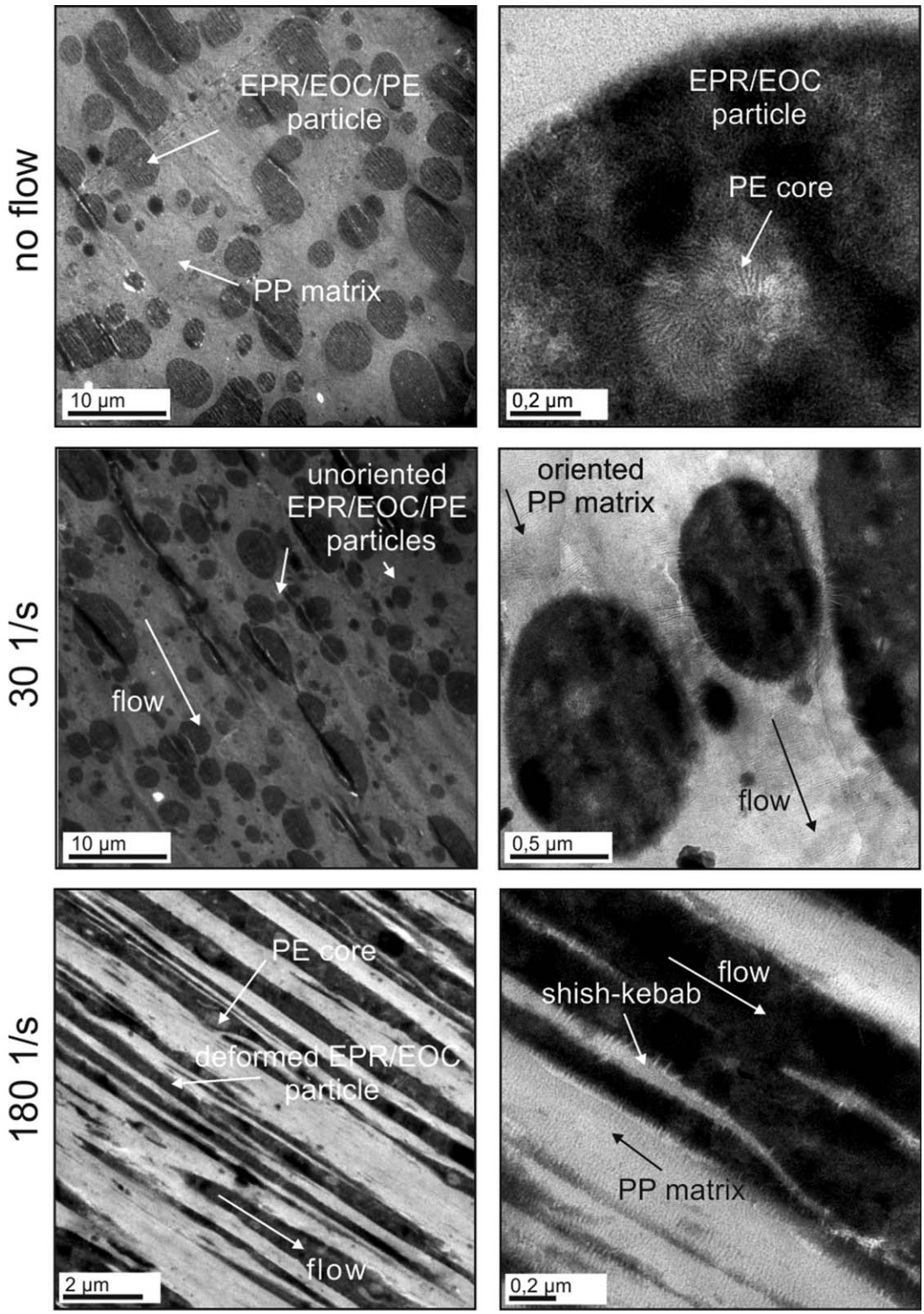

Figure 10. TEM micrographs of the morphology after solidification without flow (top), with intermediate flow (middle) and strong flow (bottom) of the EP/EPR/EOC material in low detail (left column) and high detail (right column). PE inclusions are found in the modifier, in which the EOC content is dissolved. With medium flow, oriented lamellae are formed, while at first, the modifier particles remain un-oriented. After strong flow conditions, the matrix and modifier are fully oriented and shish-kebab structures can be observed from the matrix.

Table II. Standard Characterization Results of the Investigated Materials

Composition			EP/EPR	EP/EPR/HDPE	EP/EPR/EOC
MFR ISO 1133	230°C/2.16 kg	(g/10 min)	8	8	8
Flexural ISO 178	Modulus	(MPa)	1303	1267	998
	Flex. strength	(MPa)	34.4	32.3	25.8
	Flex. strain	(%)	6.5	6.6	6.5
Charpy ISO 179	1eA+23°C	(kJ/m^2)	8.7	12.31	54.5
	1eA-20°C	(kJ/m^2)	3.95	4.48	7.4

more. This is in line with modification results achieved for single-phase PP grades.[26]

The mechanical behavior during homogeneous deformation, the intrinsic stress–strain response, can be measured by means of uniaxial compression tests. However, for the samples obtained from dilatometry (see previous section) such experiments are not feasible. Therefore, macroscopic phenomena such as yield stress and strain hardening were determined as function of flow strength using tensile testing. From each ring-shaped dilatometry sample, two dog-bone shaped specimen were cut. Since we do not see plastic localization during our experiments, we can interpret our data to analyze strain hardening modulus. The stress–strain response of all three materials is plotted in Figure 11 as true stress versus the neo-Hookean strain measure, $\lambda^2 - \lambda^{-1}$, to emphasize the effect of flow on strain hardening. Measurements on both specimen taken at equal flow conditions show, in most cases, good agreement. The highest stress levels during deformation were recorded for the EP/EPR base material. With the addition of HDPE, the stress level is slightly reduced, whereas it drops significantly for the material with EOC content, which is in agreement with the results obtained from the bending tests, see Table II.

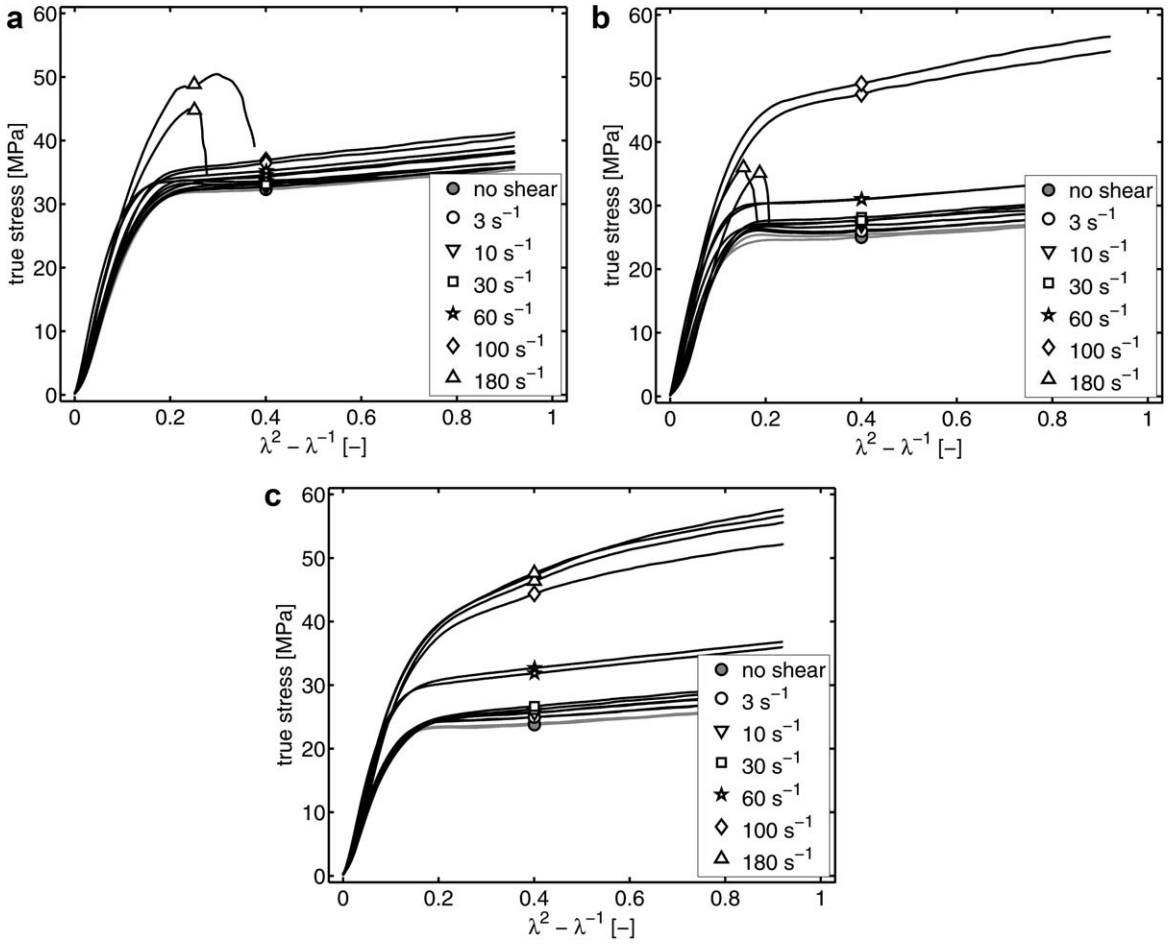

Figure 11. True stress versus strain for (a) EP/EPR, (b) EP/EPR/HDPE, and (c) EP/EPR/EOC. Markers represent the different level of shear flow during processing.

The mechanical response of the EP/EPR material in Figure 11(a) shows only a slight increase of the (yield) stress level with shear, which corresponds to the low sensitivity for flow on morphology development as observed with TEM, see Figure 6. Regarding the two compounded materials, see Figure 11(b,c), a small increase in stress was measured for the lower range of shear rates, e.g., up to 60 s^{-1}. For higher shear rate values, an increase of both the yield stress, σ_y, and strain hardening modulus, G, was measured. This is in line with earlier work on PE and polyethylene terephthalate (PET) by Schrauwen *et al.*[43] who showed that both σ_y and G are significantly affected by the level of molecular orientation present in the material as function of the processing conditions. For the materials under investigation, we can deduce that below 60 s^{-1}, no significant level of orientation is present. Indeed, only a partially oriented matrix component was observed for samples sheared at 30 s^{-1}, see Figures 8 and 10. Upon a further increase of the shear rate, enhanced orientation of the matrix occurs and ultimately, the flow strength is sufficient to also form oriented EPR inclusions, which results in an additional increase of both σ_y and G.

The different crystallization regimes can be recognized for all materials when the yield stress and strain hardening modulus are plotted versus shear rate, see Figure 12. Van Meerveld *et al.*,[44] described different crystallization regimes as function of the Weissenberg number, Wi, with $Wi=\lambda\dot{\gamma}$ and λ a characteristic relaxation time, as a measure for the strength of flow. Since here, it is not possible to define a characteristic relaxation time for the complex material composition we are studying, we use the shear rate as a measure for the flow strength. We can link the constant yield stress at low shear rates to either no influence of flow, or to a flow enhanced nucleation process within the matrix component. The molecular chains are sufficiently stretched and oriented creating extra nuclei, while the growth rate and growth-mechanism remain unaffected. As a consequence of the higher T_c caused by the flow, slightly thicker lamellae are formed which should attribute to the gradual increase of the yield stress.[45] In this case, the difference in T_c is insufficient to increase σ_y. At higher Wi numbers, high amounts of shear induced nuclei are generated and oriented crystalline structures are formed, effectively increasing σ_y and G. Using X-ray analysis, van Erp *et al.*[28] confirmed that in the first two regimes, no significant amount of molecular orientation is present, while for the final regime, highly oriented patterns can be observed typical for shish-kebab structures. Notice that the three crystallization regimes plotted in Figure 12 correspond to (I) no influence of flow or point-like nucleation, (II) flow-induced nucleation in the matrix and (III) flow-induced crystallization of the matrix (shish-kebab formation), including orientation and flow induced nucleation and oriented crystals in the rubber inclusions, respectively. Both compounded materials show a higher slope in all regions in Figure 12(a), evident for the large influence of flow as compared the EP/EPR base material.

For the EP/EPR/EOC compound σ_y is nearly equal for the two highest shear rates. This can be understood from the crystallization kinetics during and after flow which is the same, see Figure 9. Both the EP/EPR and EP/EPR/HDPE material show brittle failure for the maximum shear rate conditions. Careful observation of the deformed specimen shows that all samples failed ductile were non-transparent due to stress whitening caused by void formation. The samples obtained from the highest shear rate do not show stress-whitening. Because of the high level of orientation of the matrix and the severe deformation of the modifier content, the toughening effect of the particles is not effective any more, leading to embrittlement of the material and the absence of growing voids.

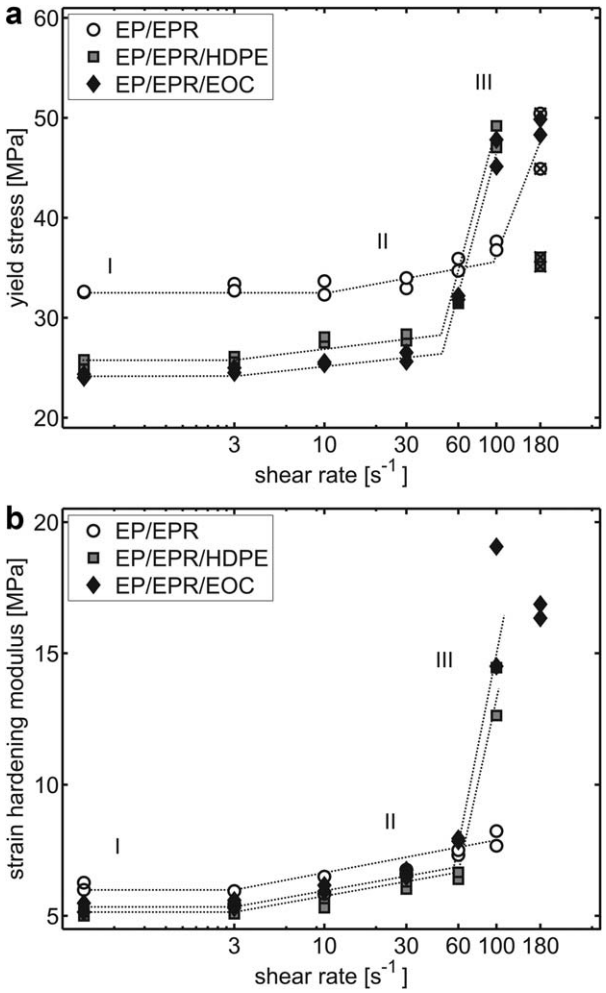

Figure 12. Effect of shear flow on (a) the yield stress and (b) strain hardening modulus for the different materials and crystallization regimes: (I) no influence of flow or point like nucleation, (II) flow induced matrix, and (III) formation of flow induced structures including oriented particles. Markers with "x" represent brittle failure.

CONCLUSION

In the present study, samples of three different heterophasic PP copolymer compositions were processed under well-controlled conditions and investigated for differences in final morphology and mechanical properties. It has been shown that for quiescent cooling conditions, crystallization of the individual material components will occur at well separated temperatures. For conditions involving flow; however, crystallization of the components may hinder or promote each other. Depending on the flow strength, here defined as the shear rate, multiple types of

morphology can be formed; the material can either remain unoriented, contain an oriented matrix component with shish-kebab structures, or become fully oriented including deformed modifier particles. The different morphology types are clearly represented in the mechanical properties, i.e., yield stress and strain hardening modulus. Regarding the final morphology and mechanical properties of the samples, both compounded materials with HDPE and EOC were most sensitive for flow. The highest flow strength investigated resulted in a high orientation of both the matrix and modifier content, with the inability of growing voids inducing brittle failure. These results clearly show the importance of the processing step for final product properties which for multi-phase materials is at least as high as for single-phase homopolymers.

ACKNOWLEDGMENTS

The authors are specifically grateful to Jingbo Wang of Borealis Polyolefine GmbH for preparation and basic characterization of the compositions. This project is supported by the Dutch Technology Foundation (STW), grant no. 07730.

REFERENCES

1. Galli, P.; Haylock, J. C. *Makromol. Chem. Macromol. Symp.* **1992**, *63*, 19.
2. Cecchin, G.; Morini, G.; Pelliconi, A. *Macromol. Symp.* **2001**, *173*, 195.
3. Grein, C.; Bernreitner, K.; Hauer, A.; Gahleitner, M.; Neißl, W. *J. Appl. Polym. Sci.* **2003**, *87*, 1702.
4. Coppola, F.; Greco, R.; Martuscelli, E.; Kammer, H. W.; Kummerlowe, C. *Polymer* **1987**, *28*, 47.
5. Gahleitner, M.; Hauer, A.; Bernreitner, K.; Ingolic, E. *Int. Polym. Process.* **2002**, *17*, 318.
6. Li, P. L.; Yi, B.; Yang, M. B. *Polym. Eng. Sci.* **2011**, *51*, 2425.
7. Chen, Y.; Ye, L. *J. Appl. Polym. Sci.* **2011**, *121*, 1013.
8. Kock, C.; Gahleitner, M.; Schausberger, A.; Ingolic, E. *J. Appl. Polym. Sci.* **2012**, *128*, 1484.
9. Bakshi, S.; Kulshreshtha, A. K.; Singh, B. P.; Anand, J. S. *Polym. Test.* **1989**, *8*, 191.
10. Gensler, R.; Plummer, C. J. G.; Grein, C.; Kausch, H. H. *Polymer* **2000**, *41*, 3809.
11. Koch, T.; Machl, D. *Polym. Test.* **2007**, *26*, 927.
12. Doshev, P.; Lach, R.; Lohse, G.; Heuvelsland, A.; Grellmann, W.; Radusch, H. J. *Polymer* **2005**, *46*, 9411.
13. Grein, C.; Gahleitner, M.; Knogler, B.; Nestelberger, S. *Rheol. Acta* **2007**, *46*, 1083.
14. Karger-Kocsis, J.; Csikai, I. *Polym. Eng. Sci.* **1987**, *27*, 241.
15. Marchal, T.; Oldenhove, B.; Daost, D.; Legras, R.; Delannay, F. *Polym. Eng. Sci.* **1998**, *38*, 2063.
16. Pantani, R.; Titomanlio, G. *J. Appl. Polym. Sci.* **2001**, *81*, 267.
17. Zhong, G. J.; Li, Z. M. *Polym. Eng. Sci.* **2005**, *45*, 1655.
18. Housmans, J. W.; Balzano, L.; Adinolfi, M.; Peters, G. W. M.; Meijer, H. E. H. *Macromol. Mater. Eng.* **2009**, *294*, 231.
19. Pantani, R.; Balzano, L.; Peters, G. W. M. *Macromol. Mater. Eng.* **2011**, *296*, 740.
20. Housmans, J. W.; Steenbakkers, R. J. A.; Roozemond, P. C.; Peters, G. W. M.; Meijer, H. E. H. *Macromolecules* **2009**, *42*, 5728.
21. Forstner, R.; Peters, G. W. M.; Rendina, C.; Housmans, J. W.; Meijer, H. E. H. *J. Therm. Anal. Calorim.* **2009**, *98*, 683.
22. van Erp, T. B.; Govaert, L. E.; Peters, G. W. M. *Macromol. Mater. Eng.* **2012**, *298*, 348.
23. Montezinos, D.; Wells, B. G.; Burns, J. L. *J. Polym. Sci.: Polym. Lett. Ed.* **1985**, *23*, 421.
24. Ward, I. M. Mechanical Properties of Solid Polymers; Wiley: New York, **1983**.
25. Bensason, S.; Minick, J.; Moet, A.; Chum, S.; Hiltner, A.; Baer, E. *J. Polym. Sci. Part B: Polym. Phys.* **1996**, *34*, 1301.
26. Kock, C.; Aust, M.; Grein, C.; Gahleitner, M. *J. Appl. Polym. Sci.* **2013**, *130*, 287.
27. van der Beek, M. H. E.; Peters, G. W. M.; Meijer, H. E. H. *Int. Polym. Process.* **2005**, *20*, 111.
28. van Erp, T. B.; Balzano, L.; Spoelstra, A. B.; Govaert, L. E.; Peters, G. W. M. *Polymer* **2013**, *53*, 5896.
29. He, J.; Zoller, P. *J. Polym. Sci. Part B: Polym. Phys.* **1994**, *32*, 1049.
30. Eder, G.; Janeschitz-Kriegl, H. Processing of Polymers. Materials Science and Technology: A Comprehensive Treatment. Wiley VCH: Weinheim, **1997**; Vol. *18*, Chapter 5, pp 269–342.
31. Stehling, F. C.; Huff, T.; Speed, C. S. *J. Appl. Polym. Sci.* **1981**, *26*, 2693.
32. Kim, G. M.; Michler, G. H. *Polymer* **1998**, *39*, 5689.
33. Zacur, R.; Goizueta, G.; Capiati, N. *Polym. Eng. Sci.* **2000**, *40*, 1921.
34. Vananroye, A.; Cardinaels, R.; van Puyvelde, P.; Moldenaers, P. *J. Rheol.* **2008**, *52*, 1459.
35. Wittmann, J. C.; Lotz, B. *Prog. Polym. Sci.* **1990**, *15*, 909.
36. Nishioa, Y.; Yamanea, T.; Takahashi, T. *J. Macromol. Sci. Part B: Phys.* **1984**, *23*, 17.
37. Zhang, X. M.; Ajji, A. *Polymer* **2005**, *46*, 3385.
38. Vanden Eynde, S.; Mathot, V. B. F.; Koch, M. H. J.; Reynaers, H. *Polymer* **2000**, *41*, 4889.
39. Reid, B. O.; Vadlamudi, M.; Mamum, A.; Janani, H.; Gao, H.; Hu, W.; Alamo, R. G. *Macromolecules* **2013**, *46*, 6485.
40. Bucknall, C. B. *Toughened Plast. Appl. Sci.* **1977**.
41. Kim, G. M.; Michler, G. H. *Polymer* **1998**, *39*, 5699.
42. Kim, G. M. PhD thesis, Martin-Luther-University, Halle-Wittenberg University, Germany, **1996**.
43. Schrauwen, B. A. G.; Breemen, L. C. A. v.; Spoelstra, A. B.; Govaert, L. E.; Peters, G. W. M.; Meijer, H. E. H. *Macromolecules* **2004**, *37*, 8618.
44. van Meerveld, J.; Peters, G. W. M.; Hütter, M. *Rheol. Acta* **2004**, *44*, 119.
45. van Erp, T. B.; Cavallo, D.; Peters, G. W. M.; Govaert, L. E. J. *Polym. Sci. Part B: Polym. Phys.* **2012**, *50*, 1438.